ТЕХНІКА ТА МЕТОДИ ЕКСПЕРИМЕНТУ
ENGINEERING AND METHODS OF EXPERIMENT

УДК 621.3.038.625+621.384.653 https://doi.org/10.15407/jnpae2024.03.289

A. G. Ponomarev*, S. V. Kolinko, V. A. Rebrov, D. V. Magilin, I. H. Ihnatiev, V. I. Voznyi, V. F. Salivon

Institute of Applied Physics, National Academy of Sciences of Ukraine, Sumy, Ukraine

*Corresponding author: ponom56@gmail.com

PERFORMANCE AND APPLICATION OF SCANNING NUCLEAR MICROPROBE AT THE INSTITUTE OF APPLIED PHYSICS OF THE NATIONAL ACADEMY OF SCIENCES OF UKRAINE[a]

The scanning nuclear microprobe of the Institute of Applied Physics of the National Academy of Sciences of Ukraine is an analytical channel based on the compact electrostatic accelerator “Sokol” of the Van de Graaff type with the maximum voltage at the high-voltage terminal of 2 MV and is designed for local non-destructive analysis of samples of various origins with high sensitivity (~1 ppm), as well as for the fabrication of three-dimensional small structures of high quality using proton beam writing. The resolution of the microprobe is about 3 μm with a beam current of I ~ 100 pA and 0.6 μm with I ~1 pA. The maximum scanning raster with a focused beam on the sample surface is 1 × 1 mm^2. The microprobe implements the techniques of particle-induced X-ray emission, Rutherford backscattering, and secondary electron microscopy. The article also gives examples of the use of the nuclear microprobe in physical research.

Keywords: electrostatic accelerator, scanning nuclear microprobe, probe forming system, proton beam writing, X-ray diffraction grating, quadrupole magnetic lens, particle-induced X-ray emission, Rutherford backscattering.

1. Introduction

Focused ion beams with energies of several mega electron volts are widely used to analyze the composition and structure of materials. Biological objects, geological materials, electronic devices, and various types of solids are studied by ion microanalysis methods [1 - 5], which have unique functions and cannot be replaced by other alternative approaches to qualitative and quantitative analysis. Spectroscopy of characteristic X-ray emission induced by accelerated ions and Rutherford backscattering spectroscopy are the most widely used methods of ion beam analysis that allow to study trace elements in materials with exceptional sensitivity and depth distribution of elements, respectively.

Focused ion beams are also used to modify materials [6 - 11]. Mechanical, electrical, magnetic, optical, and chemical properties can be modified by ion irradiation. Due to well-controlled irradiation parameters, the properties of materials can be varied precisely. This helps in the research of new materials with specific properties. The scanning nuclear microprobe is a unique facility that allows the use of micro- and nanometer-sized ion beams at sufficiently high beam currents to study materials using standard nuclear physics methods, create maps of the distribution of chemical elements in materials, and reconstruct the 3D structure of a sample.

2. Performance of the microprobe

2.1. Electrostatic accelerator

The scanning nuclear microprobe of the Institute of Applied Physics of the National Academy of Sciences of Ukraine (IAP of the NAS of Ukraine) is a channel of the analytical accelerator complex based on the compact electrostatic accelerator “Sokol” with a Van de Graaff charger. The maximum voltage at the high-voltage terminal of the accelerator is 2 MV. During its operation, the charger device and the RF ion source were modernized [12], which made it possible to increase the brightness of the proton beam four times to 7 A/m^{2}rad^{2}eV [13]. The relative energy spread of charged particles was measured on the resonant nuclear reaction of ^{27}Al(p, γ)^{28}Si and was 10^{-3}. The instability of the proton beam current in time was measured using a Faraday cup in the microprobe channel, which does not exceed 10 % [14]. The general scheme of the accelerator with a microprobe channel is shown in Fig. 1.

2.2. Scanning nuclear microprobe channel

Fig. 2 shows a schematic of the scanning nuclear microprobe channel, which shows that all the main elements such as collimators, beam line, focusing system consisting of magnetic quadrupole lens

[a] Presented at the XXXI Annual Scientific Conference of the Institute for Nuclear Research of the National Academy of Sciences of Ukraine, Kyiv, May 27 - 31, 2024.

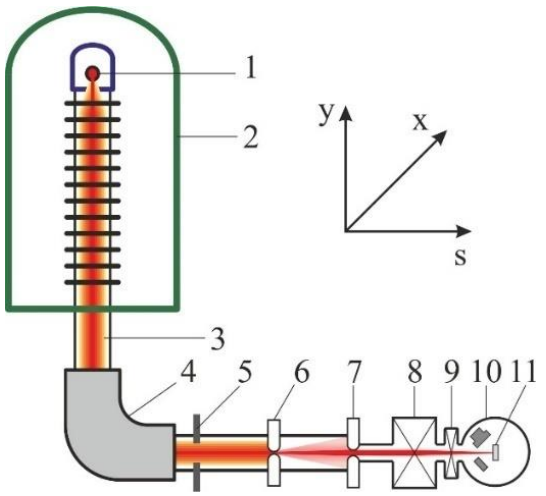

Fig. 1. Classical arrangement of elements and systems in a scanning nuclear microprobe. *1* - ion source; *2* - electrostatic accelerator; *3* - beam of accelerated ions; *4* - analyzing magnet; *5* - slit device of the beam energy stabilization system; *6* - object collimator; *7* - aperture collimator; *8* - focusing system; *9* - scanner; *10* - chamber for the interaction of the focused beam with test samples with a set of detectors; *11* - test samples. (See color Figure on the journal website.)

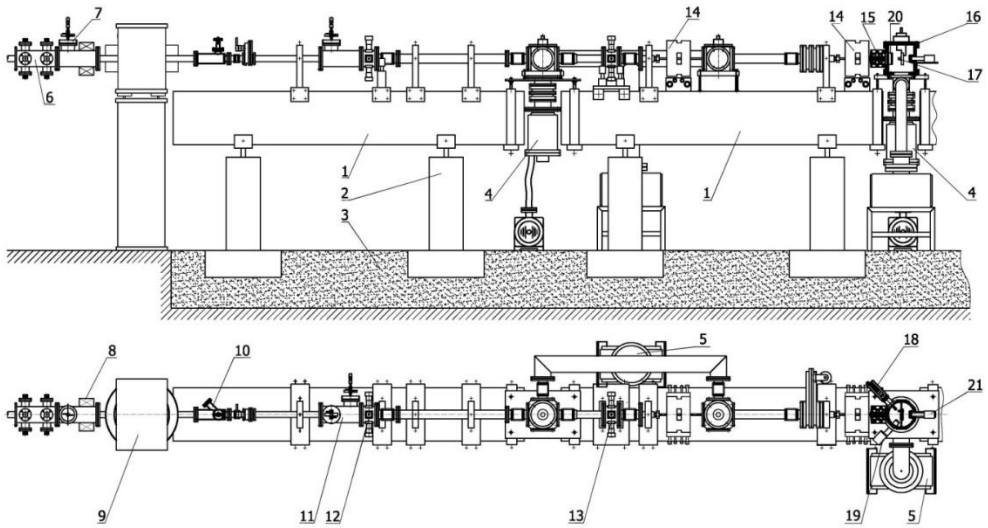

Fig. 2. Schematic of the arrangement of elements, components and systems of the probe-forming system of the scanning nuclear microprobe channel: *1* - granite girder; *2* - concrete support; *3* - sand cushion; *4* - turbomolecular pumps; *5* - ion pumps; *6* - doublet of electrostatic quadrupole lenses; *7* - vertical plane slit device; *8* - beam correction coils; *9* - switching magnet; *10* - beam visual observation camera; *11* - slit device; *12* - object collimator; *13* - aperture collimator; *14* - integrated doublet of magnetic quadrupole lenses; *15* - scanning system; *16* - chamber with test samples; *17* - sample movement mechanism; *18* - secondary electron detector; *19* – PIXE detector; *20* - Rutherford backscattering detector; *21* - optical microscope with CCD camera.

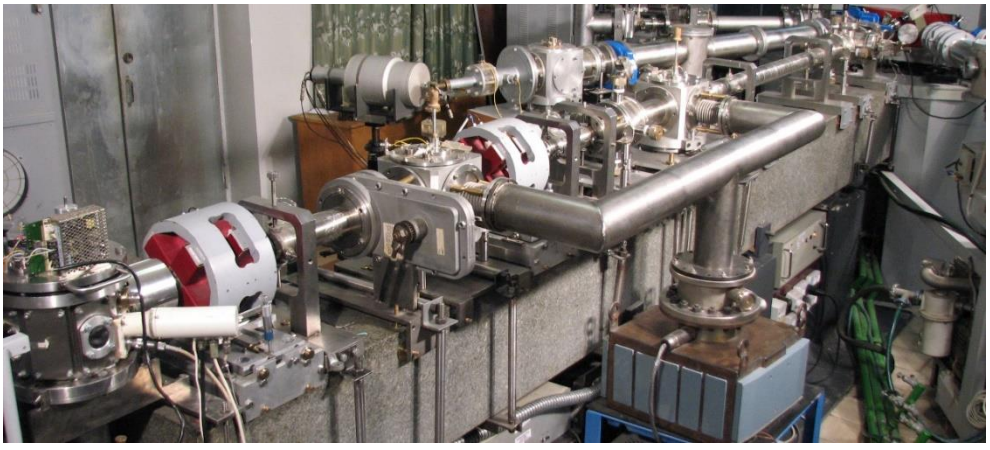

Fig. 3. General view of the scanning nuclear microprobe. (See color Figure on the journal website.)

doublets, scanner, chamber with test samples and detectors are located on granite blocks. These blocks are placed on concrete supports with a sand cushion. This avoids the influence of external vibrations. A general view of the microprobe is shown in Fig. 3.

2.3. Probe-forming system of the microprobe

Fig. 4 shows the scheme of microprobe formation. Here, using the object and aperture collimators, an initial beam volume is formed in the trajectory phase space, which must be consistent with the ion-optical properties of the focusing system, which include demagnification, spherical and chromatic aberrations. Then such a beam is formed into a microprobe on the surface of the test sample with the help of the focusing system. A separated probe-forming system is implemented in the microprobe channel, in which magnetic quadrupole lenses are combined into doublets and spaced at a certain distance a_3. This makes it possible to increase the demagnification of the focusing system with its short length. Geometric dimensions of the microprobe channel: length of the probe-forming system l = 3.85 m; working distance g = 0.235 m; distance between the boundaries of the effective fields of magnetic quadrupole lenses in doublets $a_2 = a_4$ = 0.04 m; length of the effective field of magnetic quadrupoles $L_1 = L_4$ = 0.071 m, $L_2 = L_3$ = = 0.051 m; distance between the effective fields of lenses in doublets a_3 = 0.79 m; object distance a_0 = 1.95 m.

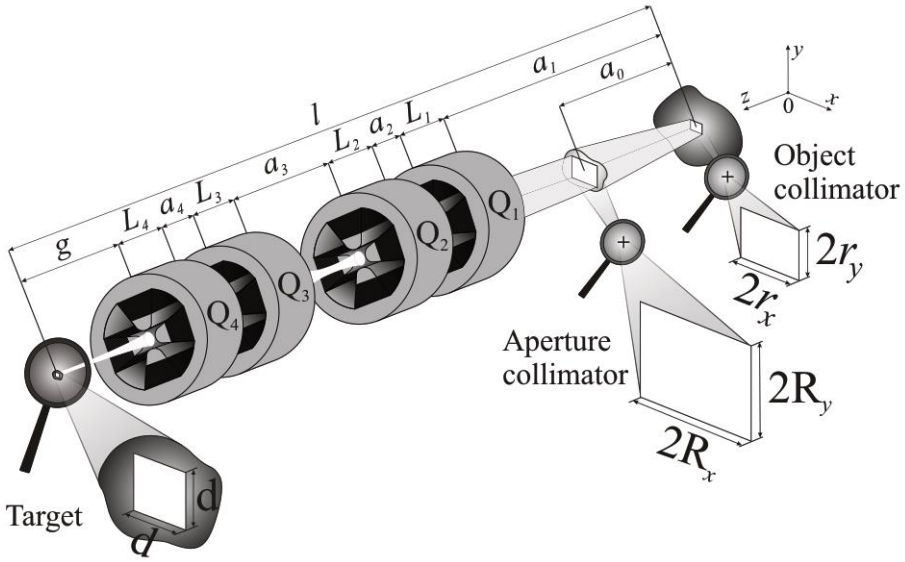

Fig. 4. Schematic of probe formation in the nuclear microprobe channel.

The basic probe-forming system in the microprobe is based on a separated orthomorphic quadruplet of magnetic quadrupole lenses [12, 15 - 17]. In this system, two independent power supplies are used to excite the quadrupole lenses according to the C1D2C2D1 scheme. Here C means that the lens is convergent in the *xOz* plane and divergent in the *yOz* plane, D, on the contrary, is a lens divergent in the *xOz* plane and convergent in the *yOz* plane, the number indicates to which power supply the lens is connected. Such a system has a small demagnifications of $D_x = D_y = D$ = 23.5, which is the same in both directions. To increase the demagnifications, we studied the probe-forming systems with four independent power supplies, where each lens is excited separately [18 - 20]. For the C1D2C3D4 power supply system, the demagnifications are $D_x \cdot D_y$ = 52·96. This system, compared to the basic system, has a much larger acceptance, which allows increasing the beam current without changing the spot size of the focused beam or increasing the resolution without changing the beam current. However, the disadvantage of this system is the difficulty of its adjustment, which requires much more time.

Separated probe-forming systems have significantly higher demagnifications than compact systems, but distanced quadrupole lenses are very sensitive to positioning relative to the beam axis [21]. As is known, a single quadrupole lens does not have the properties of precise adjustment, so it was proposed to manufacture integrated doublets of magnetic quadrupole lenses from a single piece of magnetically soft iron using electrical discharge machining, that made it possible to ensure the positioning accuracy of the poles of the doublet lenses to within 5 μm [22]. Such doublets allow precise lens adjustment in separated probe-forming systems. Single lenses can also be combined into a doublet or even a triplet, but this is labor-intensive and requires special equipment [23, 24]. Fig. 5 shows an integrated doublet of magnetic quadrupole lenses.

To form the initial trajectory phase volume of the beam, we use precision object and aperture collimators of the slit type of the same design, the walls of which are polished tungsten rods, the step of movement of the rods is 2 μm, the range of movement is 0 ... 4 mm. The collimator is shown in Fig. 6.

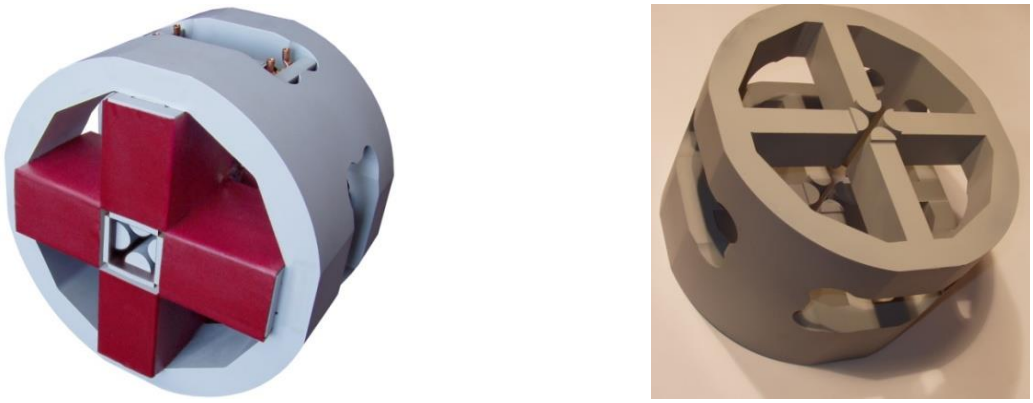

a *b*

Fig. 5. Integrated doublet of magnetic quadrupole lenses: *a* - doublet assembly; *b* - magnetic core of the doublet. (See color Figure on the journal website.)

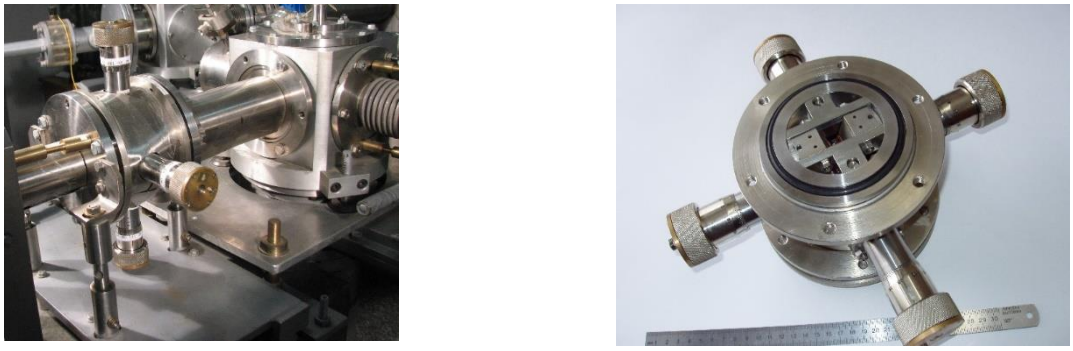

a *b*

Fig. 6 Precision slit-type collimator: *a* - aperture collimator as part of the microprobe channel; *b* - view of a separate collimator. (See color Figure on the journal website.)

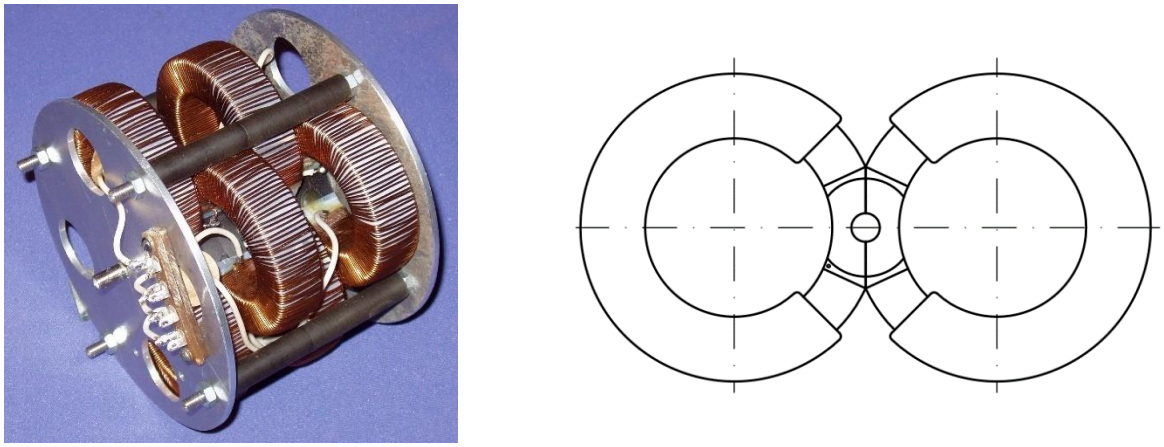

a *b*

Fig. 7. Ferromagnetic scanning system: *a* - general view of the scanning system without an external shield; *b* - dimensional drawing of one section. (See color Figure on the journal website.)

The main elements of the microprobe also include a ferromagnetic scanning system located behind the last quadrupole lens, which, on the one hand, increases the working distance and reduces the demagnifications, and on the other hand, does not lead to beam deflection in the quadrupole lenses and thus prevents aberrations from affecting the microprobe formation process. Fig. 7 shows the ferromagnetic scanning system. The scanning system is excited by a specialized power supply that allows the focused beam to be deflected in two transverse directions.

2.4. Chamber of the focused beam interaction with samples

The chamber has the shape of a rectangular octagonal prism and is made of stainless steel. Each of the side faces has connection flanges on which detecting devices, beam monitoring devices, vacuum connectors, and other systems are located. The arrangement of devices and systems is shown in Fig. 8, *a*. A general view of the chamber as part of the scanning nuclear microprobe channel is shown in Fig. 8, *b*.

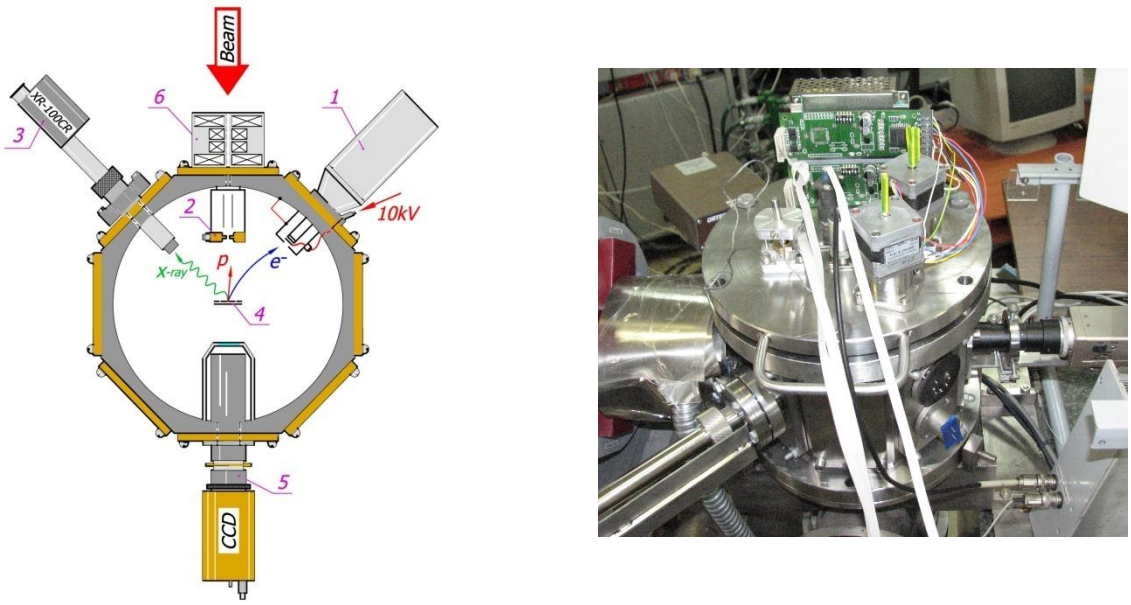

a *b*

Fig. 8. Chamber for interaction of the focused beam with samples: *a* - scheme of arrangement of devices and systems; *b* - general view of the chamber as part of the microprobe channel. (See color Figure on the journal website.)

Fig. 8, *a* illustrates:

– the block ferromagnetic scanner is mounted on the 0^o flange (pos. 6);

– the secondary electron detector is mounted on the 45^o flange (pos. 1);

– optical microscope with CCD is mounted on the 180^o flange (pos. 5);

– detector of characteristic X-rays (semiconductor detector AMTPEK® model XR-100CR with thermoelectric cooling on Peltier elements with an active crystal of 25 mm^2) is mounted on the flange 315^o (pos. 3);

– a charged particle detector (ORTEC® ring surface barrier detector, different models are available) provides registration of the backscattered particles (pos. 2).

A two-coordinate sample positioning mechanism is located on the top cover of the chamber. Stepper motors and a controller with power supplies are located on the outside (see Fig. 8, *b*). The motion is transmitted to the inside of the chamber by rotation of the vacuum-sealed rods. On the inside of the top cover of the chamber are samples on an electrically insulated holder from which the charge is collected. A ring-shaped secondary electron suppression system with a voltage of 300 V has been installed for proper charge registration.

2.5. Data acquisition system

During the experiment, it is necessary to record secondary effects in the form of induced characteristic X-rays, backscattered ions, and secondary electrons. All of this must be done in real time. Thus, each event is labeled by the position of the beam in the scan image.

A new data acquisition system [25] is currently being installed to replace the outdated microcontroller-based system. The new system is based on an NI 7852R National Instruments® Field Programmable Gate Array reconfigurable module. The module operates in real time and is connected to a personal computer via a high-speed PCI Express interface with data buffering. The system provides two main modes of operation: exposure of test areas with a specified profile and secondary electron imaging of a sample or calibration grid. Profile exposure is available in both raster and functional scan modes. Automatic calibration of the profile and scan raster scale is also implemented. The use of reconfigurable logic allows the system to be quickly adapted to the conditions of a particular experiment and the equipment available. The hardware capabilities of the scan control system allow the connection of up to 4 spectrometric ADCs for mapping the elemental composition of samples using particle-induced X-rays and ion backscattering.

2.6. Microprobe resolution

To measure the resolution of the microprobe, a standard method of scanning with a focused proton beam with an energy of 1 MeV of calibration micrometer copper grids with secondary electron imaging was used. By processing the current output profile of secondary electrons when the beam crossed the grid bar, the beam size of its full width at half maximum (FWHM) of the current density distribution was determined. The procedure for processing the secondary electron output profile is given in [26]. Fig. 9 shows the results of processing the results of scanning a micrometer copper grid with a period of

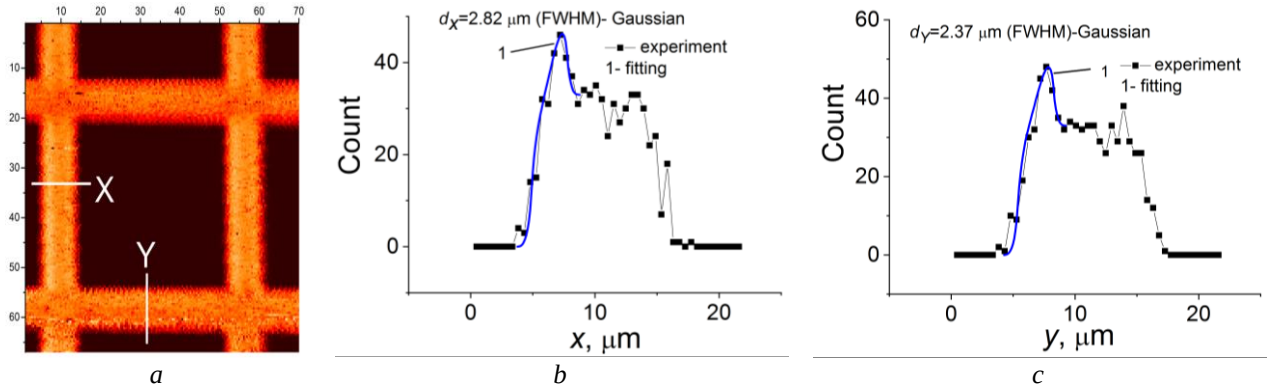

a *b* *c*

Fig. 9. *a* - secondary electrons image of a micrometer copper grid with a period of 63.5 μm; *b* and *c* - profiles of secondary electron yields at the crossing of the grid bars shown in (*a*) with processing to determine the beam size. (See color Figure on the journal website.)

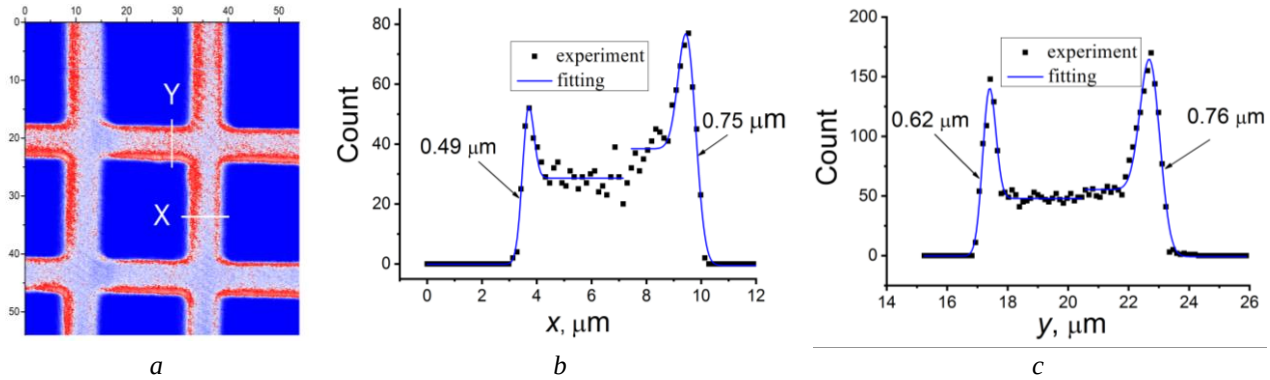

a *b* *c*

Fig. 10. *a* - secondary electrons image of a micrometer copper grid with a period of 25.4 μm; *b* and *c* profiles of secondary electron yields at the crossing of the grid bars shown in (*a*) with processing to determine the beam size. (See color Figure on the journal website.)

63.5 μm using the basic probe-forming system of a separated orthomorphic quadruplet of magnetic quadrupole lenses. This Figure shows that the achieved resolution is at the level of 3 μm at a beam current of about 100 pA.

Fig. 10 shows the processing of the secondary electron output when scanning a micrometer copper grid with a period of 25.4 μm using a probe-forming system with a separated quadruplet of magnetic quadrupoles with four power supplies. In this experiment, the beam current was at 1 pA, while the average resolution was at 0.6 μm.

3. Application of scanning nuclear microprobe in physical research

3.1. Mineralogy

Scanning nuclear microprobe was used to determine the distribution of chemical elements in geological samples of uraninites from different deposits (Ukraine, Afghanistan, and Egypt) [27, 28]. The microprobe was used due to the micrometer size of the samples, which does not require the use of a hot chamber, and the exceptional sensitivity of the method of recording characteristic X-rays induced by a focused proton beam with an energy of 1.4 MeV.

Fig. 11 shows the results of the analysis of one of the grains of the uranium-bearing mineral Ca-uraninite of Ukrainian origin. The purpose of the analysis was to determine the content of basic and impurity chemical elements. The scanning raster is 200×200 μm^2. This Figure shows the distribution of chemical elements in the scanning raster. Fig. 12 shows the spectra for the region of interest marked with a square on the SEM image. The spectra show that energy dispersive analysis on an electron microscope does not allow to identify lead inclusions, which is due to the insufficient sensitivity of this method.

The following conclusions can be drawn from this study. Using μ-PIXE, constant impurities of vanadium (0.2 - 1.0 %), iron (0.14 - 0.4 %), and copper (up to 0.13 %) were found in the studied minerals. Solid mineral inclusions of micron size were observed. Among them, the most typical was calcium phosphate with vanadium and silicon impurities. The chemical dating method has been used to determine the age of the minerals. All samples of uranium grains older than a few million years contained lead impurities (less than 1 %), distributed in the same way as uranium. This made it possible to assume the radiogenic origin of lead and to estimate the geological age

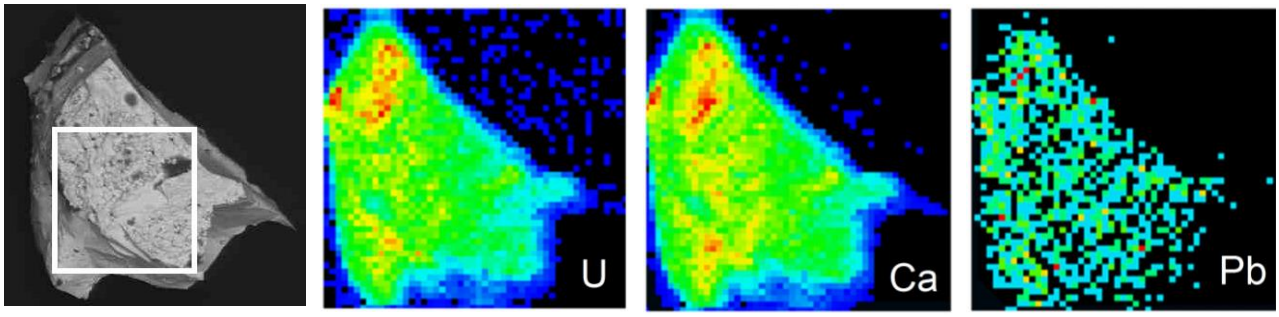

a *b* *c* *d*

Fig. 11. Image of a grain of the uranium-bearing mineral Ca-uraninite of Ukrainian origin: *a* - image by scanning electron microscope (SEM); *b*, *c*, and *d* - distribution of elements Uranium, Calcium, and Plumbum, respectively, obtained by scanning nuclear microprobe. (See color Figure on the journal website.)

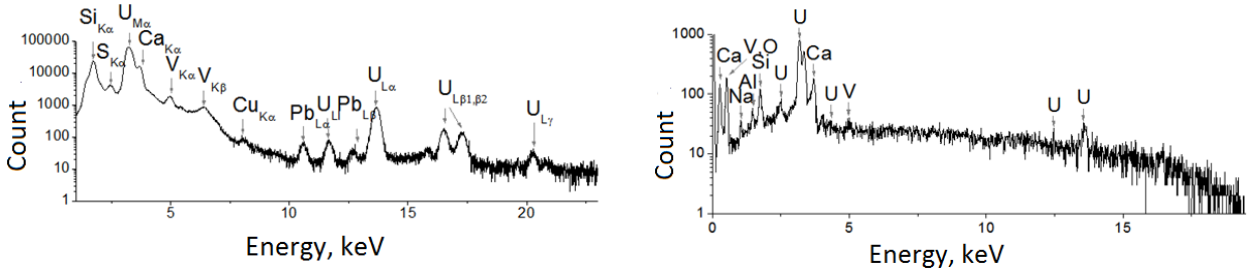

a *b*

Fig. 12. Spectra of characteristical X-ray emission with:
a - scanning nuclear microprobe; *b* – SEM.

of individual grains. The peculiarities of the trace element composition of uranium mineral grains, the phase nature of their solid impurities, and the estimates of the age of individual grains have significantly expanded the set of attributes of small uranium ore crystals that can be used, in particular, for nuclear forensics.

3.2. Nuclear energetics

In materials used in nuclear energetics, special attention is paid to the migration of impurity chemical elements along grain boundaries and in welded joints of various structures under radiation and thermal stress. Due to the high sensitivity of nuclear-physical microanalysis methods, the scanning nuclear microprobe can play a special role.

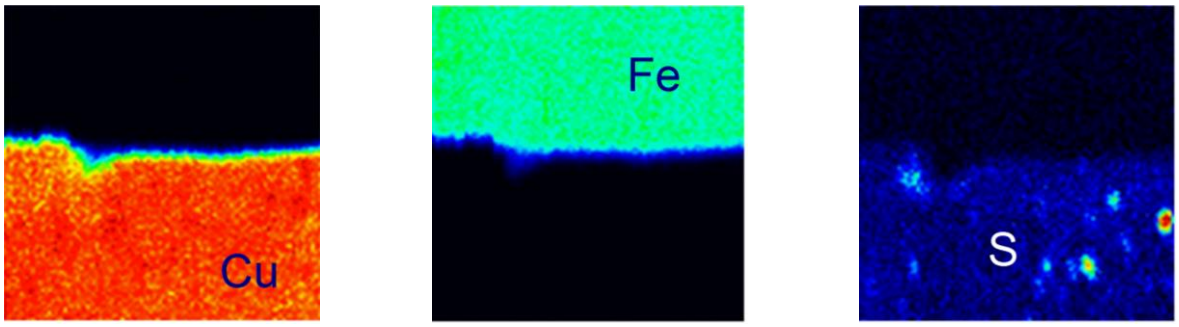

Fig. 13. Steel/copper interface (original sample). (See color Figure on the journal website.)

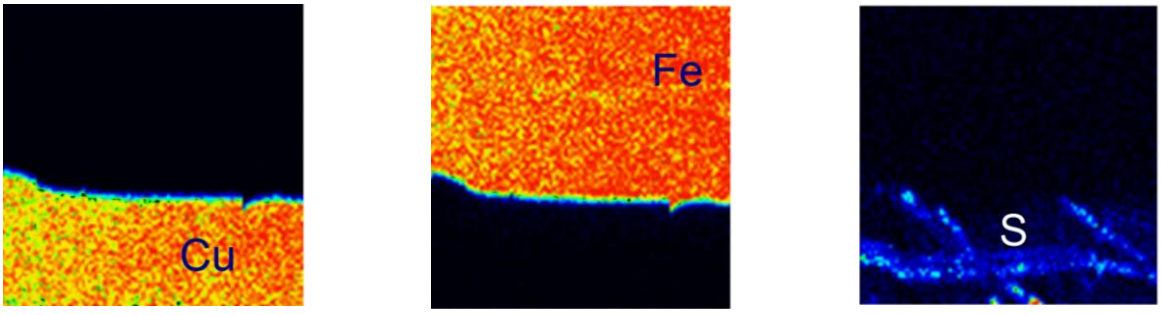

Fig. 14. Steel/copper interface (sample after cyclic heat treatment). (See color Figure on the journal website.)

Welding of stainless steels and zirconium alloys is an important technological problem in the manufacture of fuel elements for nuclear power plants. One of the methods of such welding is the use of thin layers of copper and niobium. The boundaries of the welds have been studied with a nuclear microprobe using the μPIXE method. Fig. 13 shows the distribution of elements in the original sample and Fig. 14 shows the same sample subjected to a thermal cycle. Segregation of sulfur at the grain boundaries of the copper layer can be seen.

The following conclusions can be drawn from this study. Sulfur has an increased concentration at the stainless steel/copper interface for the original sample. In the thermal cycling sample, there are noticeable changes in the stainless steel/copper interface associated with S segregation at the copper grain boundaries.

3.3. Use of proton beam writing for the fabrication of microdiffraction gratings

The IAP of the NAS of Ukraine is working on a phase-contrast X-ray setup based on an electrostatic accelerator. To produce coherent X-rays, it is necessary to fabricate X-ray diffraction gratings. For this purpose, a microprobe with a thin line focusing was used by proton beam writing [29, 30]. A thin layer of copper was deposited on the substrate, which was covered with a thin layer of polymethylmethacrylate. After irradiation with a shaped proton beam, a 3D structure is formed on the surface due to the development process, on which a lattice structure is formed after electroplating. Fig. 15 shows pilot experiments on the fabrication of X-ray microdiffraction gratings.

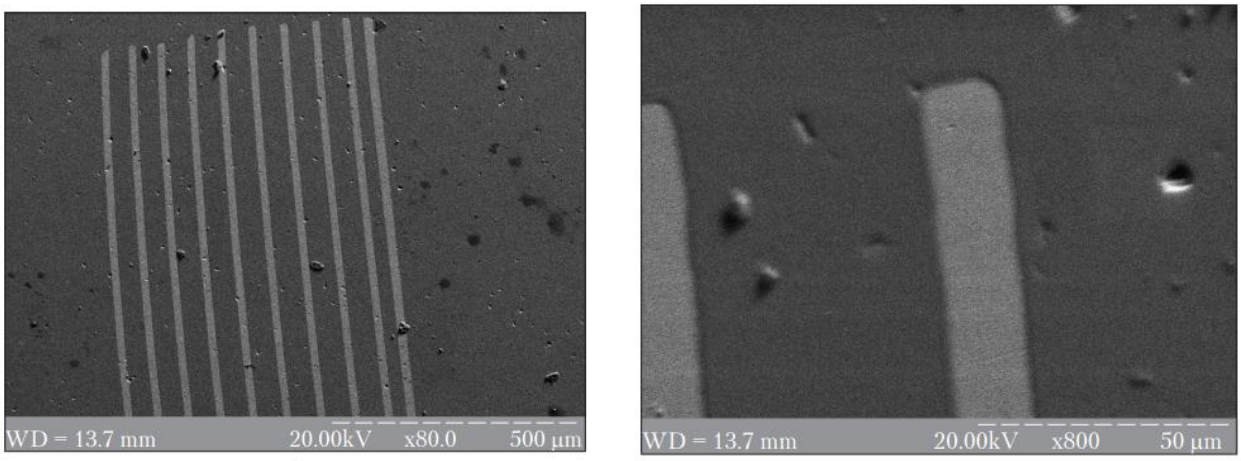

Fig. 15. Microdiffraction gratings after electroplating.

4. Conclusions

The given parameters of the accelerator and the main elements of the scanning nuclear microprobe allow us to determine the capabilities of the device. Its main feature is focused beams of light ions, which have certain advantages in the interaction with a solid in comparison with beams of electrons and low-energy heavy ions, namely, they have a very low bremsstrahlung X-rays and do not lead to the destruction of test samples. Examples of microprobe application in mineralogy, nuclear energy, and the fabrication of small-sized 3D structures are shown by far from the complete list of physical studies, which include the study of the defective structure of semiconductors by the method of ion beam induced charge (IBIC), the study of biological objects by scanning transmission ion microscopy (STIM), the determination of defects in crystals by the channeling method, etc.

REFERENCES

1. R. Meesat et al. Micro-PIXE study of metal loss from dental amalgam. Nucl. Instrum. Meth. B 404 (2017) 106.
2. S. Matsuyama et al. Current status of the Tohoku microbeam system at Tohoku University and other facilities. Nucl. Instrum. Meth. B 539 (2023) 79.
3. J. Cruz et al. Surface analysis of corroded XV-XVI century copper coins by μ-XRF and μ-PIXE/μ-EBS self-consistent analysis. Materials Characterization 161 (2020) 110170.
4. V. Nxumalo et al. Micro-PIXE characterisation of uranium occurrence in the coal zones and the mudstones of the Springbok Flats Basin, South Africa. Nucl. Instrum. Meth. B 404 (2017) 114.
5. P. Vavpetič et al. Elemental distribution and sample integrity comparison of freeze-dried and frozen-hydrated biological tissue samples with nuclear microprobe. Nucl. Instrum. Meth. B 348 (2015) 147.
6. F. Picollo et al. Realization of a diamond based high density multi electrode array by means of Deep Ion Beam Lithography. Nucl. Instrum. Meth. B 348 (2015) 199.

7. E. Ebraert et al. Deep proton writing of high aspect ratio SU-8 micro-pillars on glass. Nucl. Instrum. Meth. B 389-390 (2016) 5.
8. F. Picollo et al. Fabrication of monolithic microfluidic channels in diamond with ion beam lithography. Nucl. Instrum. Meth. B 404 (2017) 193.
9. J. Gong et al. All-silicon subwavelength structural coloration fabricated through proton beam writing and reactive ion etching. Nucl. Instrum. Meth. B 469 (2020) 52.
10. I. Rajta et al. Si micro-turbine by proton beam writing and porous silicon micromachining. Nucl. Instrum. Meth. B 267 (2009) 2292.
11. S. Ditalia Tchernij et al. A multi-electrode two-dimensional position sensitive diamond detector. Appl. Phys. Lett. 124 (2024) 223502.
12. V.E. Storizhko et al. The Sumy scanning nuclear microprobe: Design features and first tests. Nucl. Instrum. Meth. B 260 (2007) 49.
13. A.A. Ponomarov, V.I. Miroshnichenko, A.G. Ponomarev. Influence of the beam current density distribution on the spatial resolution of a nuclear microprobe. Nucl. Instrum. Meth. B 267 (2009) 2041.
14. D.V. Magilin et al. Performance of the Sumy nuclear microprobe with the integrated probe-forming system. Nucl. Instrum. Meth. B 267 (2009) 2046.
15. V.A. Brazhnik et al. Numerical optimization of magnetic nonlinear quadrupole systems in an ion microprobe with given spot size on the target. Nucl. Instrum. Meth. B 104 (1995) 92.
16. V.A. Brazhnik et al. Optimization of magnetic quadrupole probe forming systems based on separated Russian quadruplet. Nucl. Instrum. Meth. B 174 (2001) 385.
17. A.G. Ponomarev et al. Resolution limit of probe-forming systems with magnetic quadrupole lens triplets and quadruplets. Nucl. Instrum. Meth. B 201 (2003) 637.
18. A.A. Ponomarova et al. One-stage probe-forming systems with quadrupole lenses excited by individual power supplies. Nucl. Instrum. Meth. B 269 (2011) 2202.
19. K.I. Melnik, D.V. Magilin, A.G. Ponomarev. Experimental results of microprobe focusing by quadruplet with four independent lens power supplies. Nucl. Instrum. Meth. B 306 (2013) 17.
20. A.A. Ponomarova et al. The precision proton beam formation in the probe system with individual power supplies of magnetic quadrupole lenses (experimental results). Journal of Nano- and Electronic Physics 5(1) (2013) 01030. (Rus)
21. S.V. Kolinko, A.G. Ponomarev. Effect of magnetic quadrupole lens alignment on a nuclear microprobe resolution. Nucl. Instrum. Meth. B 373 (2016) 110.
22. V.A. Rebrov et al. The new design of magnetic quadrupole lens doublet manufactured from a single piece. Nucl. Instrum. Meth. B 260 (2007) 34.
23. O.S. Lapin et al. Precise centering method for triplet of magnetic quadrupole lenses using single rigid frame. Nucl. Instrum. Meth. B 404 (2017) 41.
24. A.G. Ponomarev et al. The new Sumy nuclear microprobe with single-stage quintuplet lens system. Nucl. Instrum. Meth. B 456 (2019) 21.
25. S.V. Kolinko et al. Beam scanning controller for proton-beam writing. East European Journal of Physics 3 (2021) 134.
26. A.G. Ponomarev, A.A. Ponomarov. Beam optics in nuclear microprobe: A review. Nucl. Instrum. Meth. B 497 (2021) 15.
27. A.A. Valter et al. Evaluation of a calcium-rich uraninite composition by electron and proton microprobe. Mineralogical Journal (Ukraine) 35(3) (2013) 48.
28. A.A. Valter et al. Spatial investigation of some uranium minerals using nuclear microprobe. Physics and Chemistry of Minerals 45 (2018) 533.
29. A.G. Ponomarev, V.A. Rebrov, S.V. Kolinko. Proton beam writing device based on electrostatic accelerator for 3D micro- and nano-structures fabrication. Science and Innovation 15(4) (2019) 55.
30. A.G. Ponomarev et al. Using of proton beam writing techniques for fabrication of micro diffraction gratings. Problems of Atomic Science and Technology 4(116) (2018) 285.

О. Г. Пономарьов*, С. В. Колінько, В. А. Ребров, Д. В. Магілін, І. Г. Ігнатьєв, В. І. Возний, В. Ф. Салівон

Інститут прикладної фізики НАН України, Суми, Україна

*Відповідальний автор: ponom56@gmail.com

ХАРАКТЕРИСТИКА ТА ЗАСТОСУВАННЯ СКАНУЮЧОГО ЯДЕРНОГО МІКРОЗОНДА В ІНСТИТУТІ ПРИКЛАДНОЇ ФІЗИКИ НАН УКРАЇНИ

Скануючий ядерний мікрозонд в Інституті прикладної фізики НАН України є аналітичним каналом на базі компактного електростатичного прискорювача «Сокіл» типу Ван де Грааф з максимальною напругою на високовольтному терміналі 2 МВ і призначений для локального неруйнівного аналізу зразків різного походження з високою чутливістю (~1 ppm), а також для виготовлення тривимірних малорозмірних структур високої якості за допомогою протонно-променевої літографії. Роздільна здатність мікрозонда становить близько 3 мкм зі струмом пучка I ~ 100 пА і 0,6 мкм з I ~ 1 пА. Максимальний растр сканування сфокусованим пучком по поверхні зразка 1 × 1 мм^2. У мікрозонді реалізовано методики характеристичного рентгенівського випромінювання, Резерфордівського зворотного розсіювання та вторинної електронної мікроскопії. У статті також наведено приклади застосування ядерного мікрозонда у фізичних дослідженнях.

Ключові слова: електростатичний прискорювач, скануючий ядерний мікрозонд, зондоформуюча система, протонно-променева літографія, рентгенівська дифракційна решітка, квадрупольна магнітна лінза, характеристичне рентгенівське випромінювання, Резерфордівське зворотне розсіювання.

Надійшла / Received 19.06.2024